

SCIENTIFIC REPORTS



OPEN

Hybrid Printing Metal-mesh Transparent Conductive Films with Lower Energy Photonically Sintered Copper/tin Ink

Xiaolian Chen^{1,2}, Xinzhou Wu², Shuangshuang Shao², Jinyong Zhuang², Liming Xie², Shuhong Nie², Wenming Su², Zheng Chen² & Zheng Cui²

With the help of photonic sintering using intensive pulse light (IPL), copper has started to replace silver as a printable conductive material for printing electrodes in electronic circuits. However, to sinter copper ink, high energy IPL has to be used, which often causes electrode destruction, due to unreleased stress concentration and massive heat generated. In this study, a Cu/Sn hybrid ink has been developed by mixing Cu and Sn particles. The hybrid ink requires lower sintering energy than normal copper ink and has been successfully employed in a hybrid printing process to make metal-mesh transparent conductive films (TCFs). The sintering energy of Cu/Sn hybrid films with the mass ratio of 2:1 and 1:1 (Cu:Sn) were decreased by 21% compared to sintering pure Cu film, which is attributed to the lower melting point of Sn for hybrid ink. Detailed study showed that the Sn particles were effectively fused among Cu particles and formed conducting path between them. The hybrid printed Cu/Sn metal-mesh TCF with line width of 3.5 μm , high transmittance of 84% and low sheet resistance of 14 Ω/\square have been achieved with less defects and better quality than printed pure copper metal-mesh TCFs.

Printed electronics is a new emerging field in recent years^{1,2}. Compared with conventional vacuum deposition and photolithographic techniques, printing is low-cost, efficient for material usage^{3,4}, has been applied to fabricated flexible displays, radio frequency identification tags (RFID)^{5,6}, and wearable electronics^{7,8}.

Conductive ink based on silver nanoparticle is widely used in printed electronics^{9,10}, albeit at high cost¹¹. There have been continuous efforts in developing copper ink, either based on copper or copper oxide nanoparticles, because of the low price of copper. However, copper nanoparticles are too easily to oxidize and cannot be sintered by traditional sintering methods under ambient condition^{12,13}. The photonic sintering using intensive pulse light (IPL) has proved to be effective for copper nanoparticle ink^{14,15}. However, the high photonic sintering energy, which is needed to make copper nanoparticle films conductive, leads to the destruction of samples¹⁶.

One of the important applications of conductive inks is to print conductive electrodes. There has been a considerable surge of activity in the development of printing metal grids as an alternative to ITO for transparent conductive films (TCFs)^{17–20}. Among the many reported techniques, the authors' group developed a hybrid printing process which prints conductive ink into a narrow trench instead of conventionally on surface (The hybrid printing process is shown in Supplementary Fig. S1). In this innovative process, less than 3 μm grid width can be achieved and the embedded Ag metal-mesh TCF has extremely low sheet resistance ($<0.5 \Omega/\square$) while still maintains high transparency ($>85\%$)²¹. The hybrid printed TCFs have been successfully used in touch-screen panels and solar cells^{21–23}. The authors' group also conducted research on copper ink and used an IPL for photonic sintering²⁴. Unlike Ag ink, Cu ink usually needs very high energy photonic sintering to convert copper oxide into copper. Though high energy photonic sintering poses no problem for copper ink printed on a flat surface, it is problematic if the copper ink is embedded into a trench. Defects in the forms of broken mesh lines and missing copper materials in the trenches happened in the process.

¹School of Nano-Tech and Nano-Bionics, University of Science and Technology of China, Hefei, 230026, People's Republic of China. ²Printable Electronics Research Centre, Suzhou Institute of Nano-Tech and Nano-Bionics, Chinese Academy of Sciences, Suzhou, 215123, People's Republic of China. Correspondence and requests for materials should be addressed to W.S. (email: wmsu2008@sinano.ac.cn) or Z.Ch. (email: zchen2007@sinano.ac.cn)

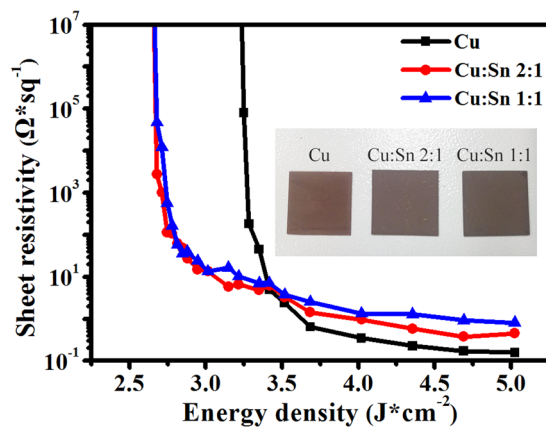


Figure 1. Sheet resistance of Cu and Cu/Sn film (2:1 and 1:1) with respect to different sintered energy density of 2.64 to 5.02 J/cm², (inset) the sintered screen-printed metal films.

In this study, a Cu/Sn hybrid ink has been developed by mixing Cu and Sn particles. The sintered energy of Cu/Sn film with mass ratio of 2:1 (Cu:Sn) was found 21% less than that for Cu film, which is attributed to the lower melting point of Sn for hybrid ink. The SEM inspection revealed that the molten Sn particles were fused among Cu particles and formed conducting paths on Cu/Sn hybrid film. Using the Cu/Sn ink and previously developed Cu ink at the authors' group for comparison, metal-mesh TCFs were fabricated by the hybrid printing process and sintered with an IPL. The Cu/Sn metal-mesh TCF achieved the transmittance of 84% and low sheet resistance of 14 Ω/□ with less defects and better quality than printed pure copper metal-mesh TCFs.

Results

Photonic sintering of screen-printed Cu and Cu/Sn films. In order to study the sintering characteristics of Cu/Sn hybrid film and to compare with the sintering of pure Cu film, the Cu and Cu/Sn films with the size of 2 cm * 2 cm (as shown in the inset of Fig. 1) were fabricated by screen-printing and the IPL energy density ranging from 2.64 to 5.02 J/cm² was applied. Figure 1 presented the sheet resistance of sintered Cu and Cu/Sn hybrid film with respect to irradiation energy. Cu/Sn films of mass ratio 2:1 and 1:1 (Cu:Sn) sintered by 2.68 J/cm² exhibited weak conductivity. And sheet resistance was rapidly down with the increase of sintered energy density. However, the Cu film was non-conductive until sintered by 3.25 J/cm². It implied that the sintering energy density of Cu/Sn hybrid films at the mass ratio of 2:1 and 1:1 was about 21% lower than that of Cu film in order to achieve conductivity. It was also observed that the Cu/Sn films reached to the lowest and stable sheet resistance (2:1: 0.379 Ω/□, 1:1: 0.808 Ω/□) when energy was higher than 3.25 J/cm²; but Cu film only moved towards flatness after 3.65 J/cm² and had the lowest sheet resistance of 0.158 Ω/□. The thickness of Cu and Cu/Sn films was analyzed by step profiler (Supplementary Fig. S6). The data presented that Cu and Cu/Sn films before sintering had the similar average thickness, about 6 μm. Meanwhile, the thickness of the Cu and Cu/Sn films decreased to ~5 μm after the 4.69 J/cm² flash light-sintering process.

Generally, electrical resistance of films made by particle ink is dependent on the intrinsic resistance of metal and contact resistance between metal particles^{25,26}. Before sintered by IPL, the surface of spherical Cu and Sn particles were covered by insulating PVP layer and electric charge could not hop into adjacent particles, resulting in non-conductivity in Cu and Cu/Sn films. Figure 2 are the SEM images of Cu and mixed Cu/Sn films before and after sintering by IPL. The top row images (a, b, c) are pure Cu ink, the central row (d, e, f) a 2:1 mixture and the bottom row (g, h, i) a 1:1 mixture. The left column (a, d, g) correspond to samples before sintering, those in the central column (b, e, h) to 3.25 J/cm² and those in the right column (c, f, i) to 4.69 J/cm². At low photonic energy, Sn particles started to melt because of its low melting point (the bulk Sn is 231.89 °C)²⁷ and to connect with Cu particles (Fig. 2e,h). Simultaneously, PVP at the surface of particles was decomposed partially and became thinner²⁸, as described in schematic diagram of Fig. 3. The charges were able to transport more easily through the interface between Cu particles than that for Cu film, so was the better conductivity of Cu/Sn films than Cu films under the low energy. As the sintering energy density increased, Sn particles were melt completely and Cu particles covered by PVP were also gradually reduced to pure Cu (Fig. 2f,i). The barrier of charge transport between particles for Cu/Sn films was further reduced. Meanwhile, sintered Cu particles on pure Cu film were also connected with each other¹⁴, so that the charge of Cu film could transport between the melt Cu particles just like the bulk Cu. Owing to the greater conductivity of bulk Cu (1.68 μΩ·cm) than bulk Sn (10.1 μΩ·cm)^{27,29}, the conductivity of Cu film sintered by higher energy density were better than Cu/Sn particle ink films, as shown in Fig. 1. Figure S7 in Supplementary Information showed the EDS mapping images of Cu/Sn film (1:1) before and after sintering, which are provided in the Cu (green) and Sn (red) distribution. These images confirmed that the Cu/Sn ink was well-distributed.

In order to verify that oxidized Cu particles were reduced to pure Cu particles at the high energy density of 4.69 J/cm², XPS analysis before and after sintering were conducted. As showed in Fig. 4a,b, curve fitting with Gaussian function divided Cu 2p_{3/2} region with two peaks around 932.6 eV and 934.6 eV, which resulted from Cu and CuO, respectively³⁰. Before sintering, there was a small Cu 2p_{3/2} peak around 934.6 eV (Fig. 4a). But Cu 2p_{3/2} peak around 934.6 eV nearly disappeared after sintering of 4.69 J/cm² (Fig. 4b), manifesting CuO did not exist on

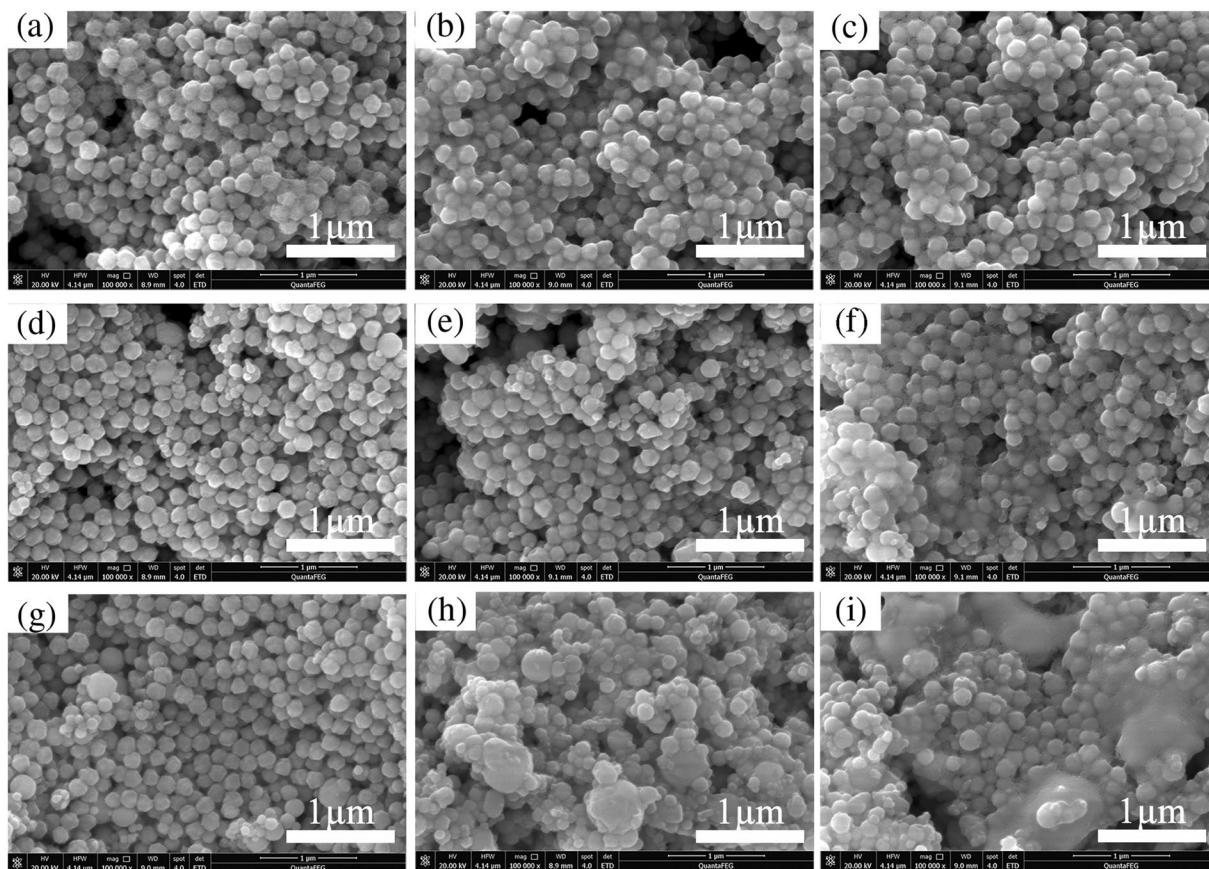


Figure 2. SEM images of Cu and mixed Cu/Sn films before and after sintering by IPL. The top row images (a, b, c) are pure Cu ink, the central row (d, e, f) a 2:1 mixture and the bottom row (g, h, i) a 1:1 mixture. The left column (a, d, g) correspond to samples before sintering, those in the central column (b, e, h) to 3.25 J/cm^2 and those in the right column (c, f, i) to 4.69 J/cm^2 .

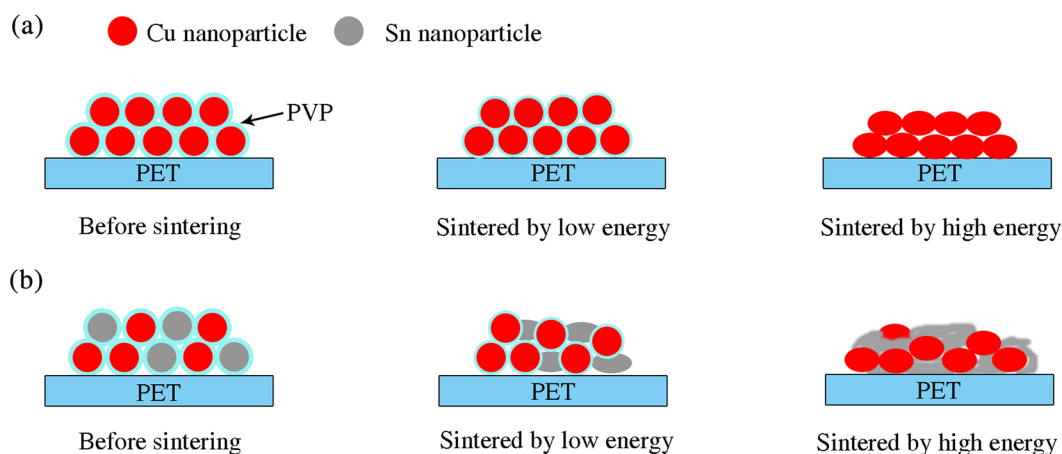


Figure 3. Sintered schematic diagram of Cu and mixed Cu/Sn films under low energy and high energy: (a) Cu ink film; (b) Mixed Cu/Sn ink film.

the surface of Cu particles and was totally reduced to Cu by the decomposition of PVP²⁸. So the Cu particles on Cu and Cu/Sn films were sintered completely by 4.69 J/cm^2 . At the same time, the XPS analysis of Sn particles was carried out to measure the surface composition (Fig. 4c,d). The Sn spectrum showed two peaks due to spin-orbital coupling of the 3d state: Sn $3d_{5/2}$ at 485 eV and Sn $3d_{3/2}$ at 493.4 eV¹¹. As shown in Fig. 4c,d, regardless of the flash light-sintering process, the Sn $3d_{5/2}$ region was divided into two peaks: one strong peak has a binding energy of 485 eV (Sn), another extremely weak peak was around 487 eV, indicating SnO_x ^{11,31}. This data indicated that Sn particles was barely oxidized during the IPL process.

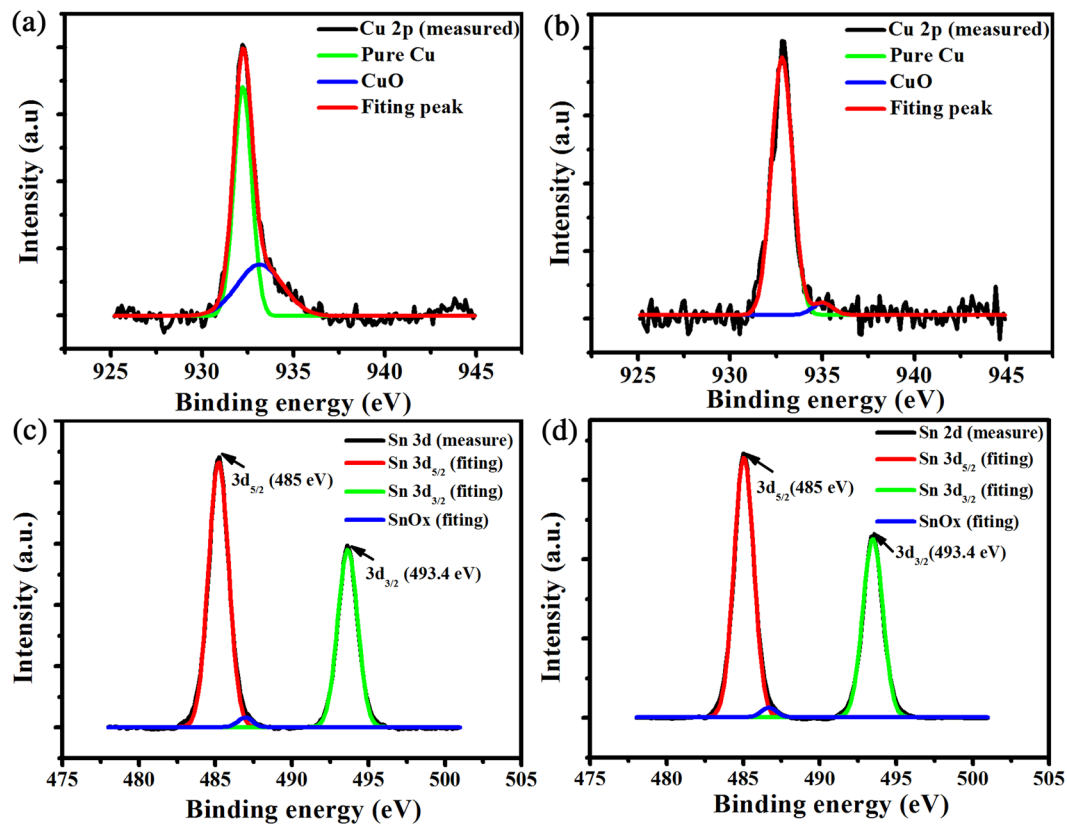


Figure 4. XPS spectra of Cu and Sn particles before and after sintering: (a) Cu and (c) Sn particles before sintering; (b) Cu and (d) Sn particles after sintered by 4.69 J/cm^2 .

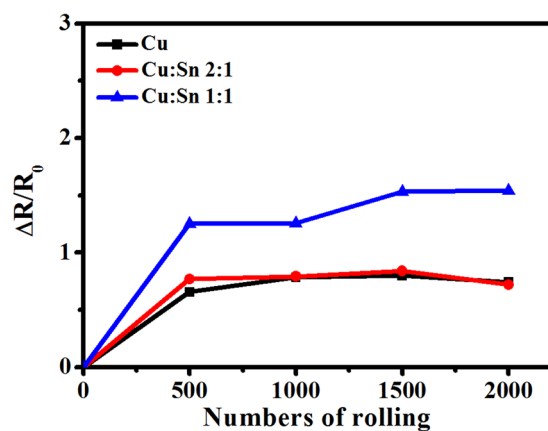


Figure 5. Rolling fatigue test results of Cu and mixed Cu/Sn films.

To compare the mechanical flexibility of sintered Cu and Cu/Sn films, rolling tests were conducted. Figure 5 presented the sheet resistance change about sintered Cu/Sn hybrid films after rolling ($\Delta R/R_0$). All the films in the rolling test were sintered at 4.69 J/cm^2 . After 500 cycles, $\Delta R/R_0$ for Cu film was 0.65 while the values for Cu/Sn hybrid films of 2:1 and 1:1 were 0.76 and 1.25, respectively, implying that the sheet resistance just changed a little and exhibited good property of mechanical stability. It was noteworthy that $\Delta R/R_0$ went up when the mass ratio of Sn in Cu ink was increased. This phenomenon was attributed to that fully melt Sn particles under high energy were fused with Cu particles together (as presented in Fig. 2i) while Cu particles for Cu film could not be fused completely (Fig. 2c). But $\Delta R/R_0$ for both films retained constant after 2000 cycles and just kept below 1.5, showing good mechanical stability.

Photonic sintering of hybrid printed Cu and Cu/Sn metal-mesh TCFs. Both the Cu and Cu/Sn ink were applied to hybrid printing of metal-mesh TCFs. Due to faster heat dissipation compared with the

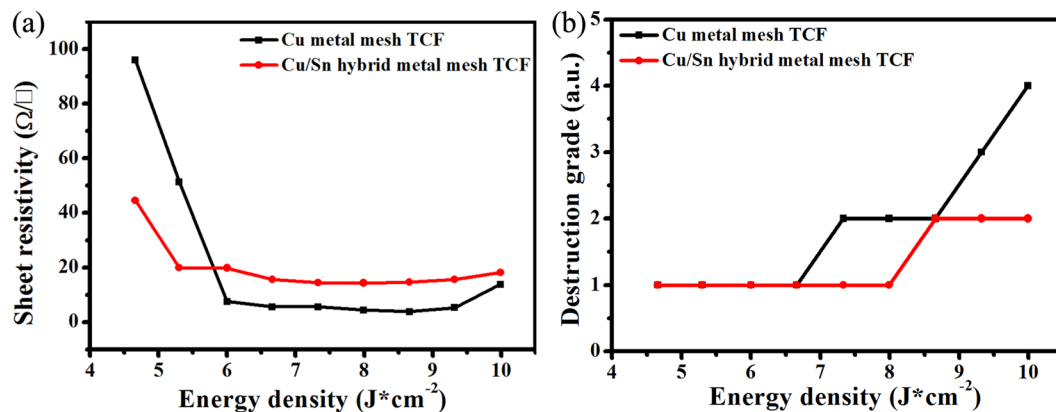


Figure 6. (a) The sheet resistance and (b) Destruction grade of Cu and Cu/Sn hybrid metal-mesh TCFs sintered by different energy intensity.

scree-printing continuous films, it was found that the higher sintering energy was needed for the narrower Cu grids (3.5 μm) of metal-mesh TCF to achieve the melting temperature of Cu particles³². As a result, the energy density of 4.66–10 J/cm^2 was applied by experimental optimization, using one pulse with fixed 2.6 kV. But many defects and fractured Cu grids were observed on Cu metal-mesh TCF (as showed in Supplementary Fig. S10) because of massive heat and stress concentration.

In contrast to the hybrid printed Cu metal-mesh, the Cu/Sn particle ink needs lower sintering energy as discussed above. Figure 6a showed the sheet resistance values plotted across the energy density of between 4.66 J/cm^2 and 10 J/cm^2 . We found that the sheet resistance was lying on the decreasing curve before 8.66 J/cm^2 . And Cu metal-mesh TCF, which had the transmittance of about 84% at 550 nm (Supplementary Fig. S3), had the lowest sheet resistance of 3.8 Ω/\square . However, the conductivity would fall off while sintered energy was higher than 8.66 J/cm^2 . For Cu/Sn metal-mesh TCF, it reached the lowest sheet resistance of 14.5 Ω/\square when sintered by 7.33 J/cm^2 and kept almost invariable after 7.33 J/cm^2 .

Though the conductivity of hybrid printed Cu/Sn metal-mesh TCF was not as advantageous as the Cu metal-mesh TCF, the great benefit of lowering photonic sintering energy is the reduced defect level in the TCFs. To quantify the defect level of TCF, the quality of film was evaluated using a grade scheme³³. Grade 1 indicates perfectly intact structures in all parts of the test pattern. Grade 2 indicates minor fractured lines. Grade 3 indicates destructive lines and structures below 5% of the whole area. Grade 4 indicates destructive lines and structures at 5% to 20% of the whole area. Grade 5 indicates major damage that make it difficult to measure the sheet resistance. The optical microscope images for different grades were exhibited in Supplementary Fig. S11.

Figure 6b exhibited the relationship between the film grade and sintering energy. Cu metal-mesh TCF do not show any damage before sintering energy density of 6.66 J/cm^2 . After 7.33 J/cm^2 , the structure showed some damages, and the higher energy density was, the more significant the destruction was. For Cu/Sn metal-mesh TCF (1:1), it displayed excellent film quality before 7.99 J/cm^2 and just a slight damage after 8.66 J/cm^2 . Figure 7 also presented the optical microscopic images of Cu and Cu/Sn metal-mesh TCF sintered by 7.99 J/cm^2 . The plastic substrate for Cu metal-mesh TCF was deformed and Cu lines in the trenches were broken while Cu/Sn metal-mesh TCF exhibited perfectly intact structure. The much reduced damage was probably the result that the melting of Sn particles consumed additional heat, limiting the maximum temperature. The DSC was analyzed for particles to support the speculation. As shown in Supplementary Fig. S9, the DSC curves of Sn and mixed Cu/Sn ink presented the endothermic peak around 230 °C while it did not exist in the Cu ink, which means that the Cu metal-mesh TCF has higher instantaneous temperature than Cu/Sn metal-mesh TCF under the same condition, causing unreleased massive stress^{32,34–37}. On the other hand, the melting of Sn particles around Cu particles played the role of releasing part of stress caused by momentary temperature. Consequently, Cu metal-mesh TCF was damaged more easily while Cu/Sn metal-mesh TCF was not.

Figure 8 showed the result of adhesion test on metal-mesh TCFs according to ASTM D3359 standard. Figure 8a,b presented the images of Cu metal-mesh TCF sintered by 7.99 J/cm^2 before adhesion test. After the adhesion test, most of the Cu fell off the trenches, and only 10% of Cu particles left (Fig. 8c,d), resulting in no conductivity. Figure 8e,f are the images of Cu/Sn metal-mesh TCF before adhesion test. After adhesion test, more than 90% of Cu/Sn were still in the trenches (Fig. 8g,h), resulting in the TCF still conductive at the sheet resistance of 28 Ω/\square . The Cu grids actually protruded out of the surface due to heat induced stress while there was no noticeable protruding for Cu/Sn metal-mesh TCF (Supplementary Fig. S2). As a result, stronger adhesion of Cu/Sn than Cu only metal-mesh TCF was achieved.

Discussion

A Cu/Sn hybrid ink has been developed by mixing Cu and Sn particles. The hybrid ink requires lower sintering energy than normal copper ink and has been successfully employed in a hybrid printing process to make metal-mesh transparent conductive films (TCFs). The sintering energy of Cu/Sn hybrid films with the mass ratio of 2:1 and 1:1 (Cu:Sn) were decreased by 21% compared to sintering pure Cu film, which is attributed to the lower melting point of Sn for hybrid ink. Detailed study showed that the Sn particles were effectively fused among Cu

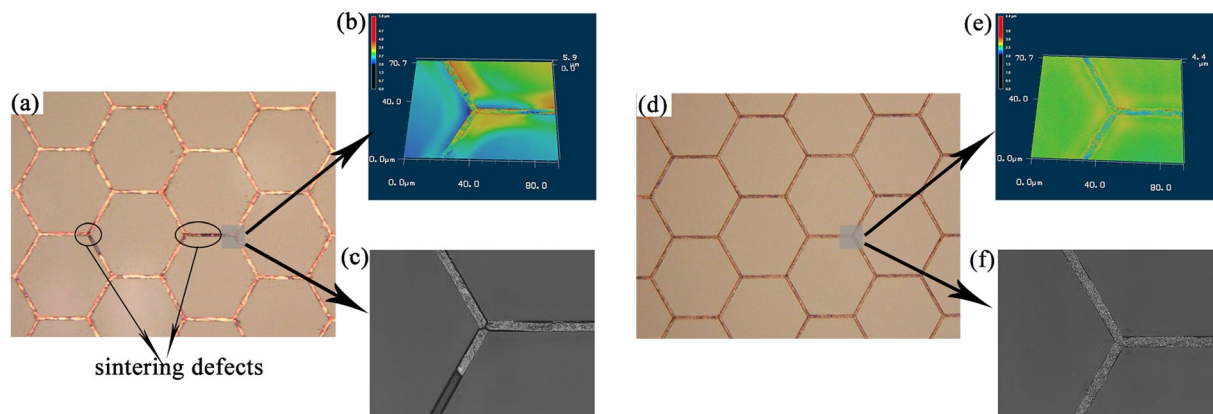


Figure 7. The optical microscope images of metal-mesh TCF sintered by 7.99 J/cm^2 : (a), (b) and (c) Cu metal-mesh TCF; (d), (e) and (f) Cu/Sn metal-mesh TCF; (a) and (d) In laser and color modes; (b) and (e) In 3D mode; (c) and (f) In laser mode.

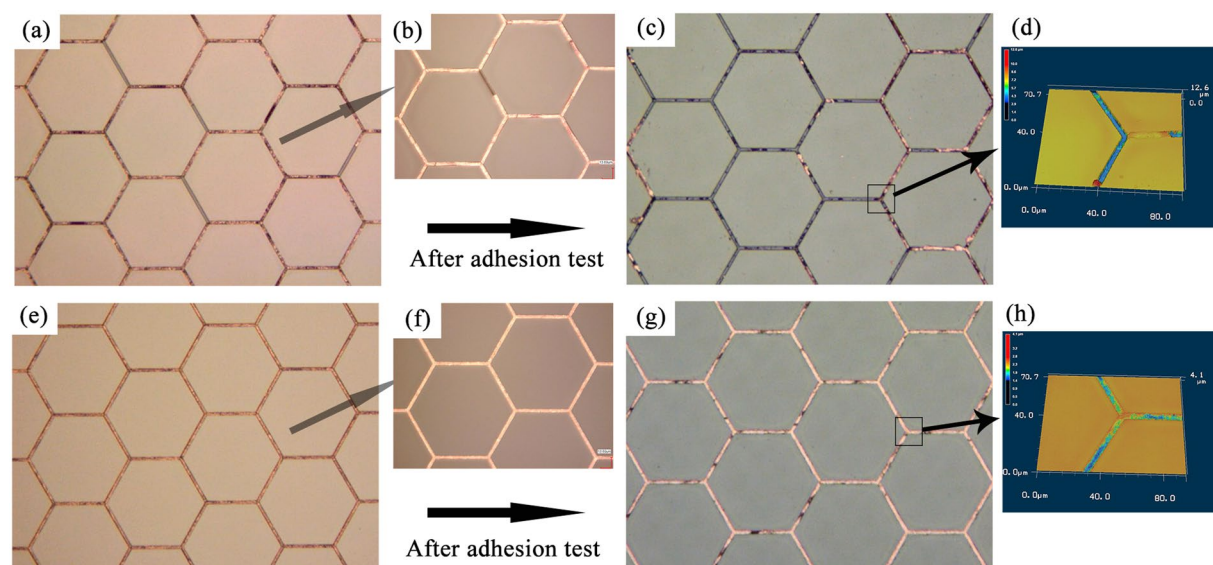


Figure 8. The optical microscope images of metal-mesh TCFs before and after adhesion test: the top row of images showed Cu metal-mesh TCF sintered by 7.99 J/cm^2 ; the bottom row showed Cu/Sn metal-mesh TCF; (a), (b), (e) and (f) before adhesion test; (c), (d), (g) and (h) after adhesion test.

particles and formed conducting path between them. The hybrid printed Cu/Sn metal-mesh TCF with line width of $3.5 \mu\text{m}$, high transmittance of 84% and low sheet resistance of $14 \Omega/\square$ have been achieved with less defects and better quality than printed pure copper metal-mesh TCFs.

Methods

Preparation of Cu/Sn hybrid inks. To fabricate Cu/Sn hybrid inks, commercially available Cu particles with oxide shells ($150 \text{ nm} \pm 30 \text{ nm}$ in diameter, oxide thickness $< 3 \text{ nm}$; Suzhou NanoGrid Technology Co. Ltd) and Sn particles ($100\text{--}300 \text{ nm}$ in diameter; Sigma-Aldrich) were used in this study, as shown in Supplementary Fig. S4. Polyvinyl pyrrolidone (PVP, Mw 44000–54000) as the capping agent and ethyl cellulose used as adhesion agent were purchased from Sinopharm chemical reagent Co. Ltd. And Cu and Sn particles were dispersed in a mixed solvent containing 10 g of terpineol, 1 g of PVP and 0.6 g of ethyl cellulose to fabricate Cu ink and Sn ink, respectively. Then Cu ink was mixed with different mass of Sn ink by stirring for 30 min, followed by ball milling for 8 h. Cu/Sn hybrid inks have different mass ratios of Cu to Sn, about 1:0, 2:1 and 1:1, respectively, as showed in Table 1.

Sintering of Cu and Cu/Sn hybrid ink by intensive pulse light (IPL). Cu and Cu/Sn hybrid inks were screen-printed on a polyethylene terephthalate (PET) substrate with a thickness of $188 \mu\text{m}$ to fabricate Cu and Cu/Sn hybrid films, followed by drying on a hot box at 80°C for 2 min. IPL from a xenon flash lamp system (Sinteron 2010, Xenon Corp.) was applied with A type lamp, of which wavelengths ranged from $370\text{--}800 \text{ nm}$. The

Terpilenol (g)	PVP (g)	Ethyl cellulose (g)	Cu particles (g)	Sn particles (g)	Cu:Sn
10	0.8	0.3	16.70	0.00	1:0
10	0.8	0.3	11.13	5.57	2:1
10	0.8	0.3	8.35	8.35	1:1

Table 1. Contents of formulated Cu/Sn hybrid ink.

distance from the lamp to substrate stage was 3.5 cm. The sintered energy density of Cu and Cu/Sn hybrid films from 2.68 J/cm² to 5.02 J/cm² was used with the single pulse. It was adjusted by increasing the single pulse time with constant voltage of 2.3 kV.

After sintering, the sheet resistance of Cu or Cu/Sn hybrid films was measured by four-point probe station (Suzhou Jingge Electronic Co., Ltd). The microstructure, surface and elemental mapping of films were tested by scanning electron microscopy (SEM, Quanta 400 FEG). The absorption spectra of Cu and Sn NPs were analyzed with a UV-visible spectrometer (Lambda 750, PerkinElmer). The surface profiles were analyzed by using step profiler (Dektak XT, Bruker Corporation). Differential scanning calorimetry (DSC) was performed Netzsch DSC F3 Maia (Germany) at a heating rate of 10 °C min⁻¹ from room temperature to 270 °C under a nitrogen atmosphere.

The mechanical property of sintered Cu/Sn ink films was measured by rolling radius of 10 mm; all kinds of conducting films in rolling test were sintered by 4.69 J/cm² and the sheet resistance change after rolling was determined by:

$$\Delta R/R_0 = (R - R_0)/R_0 \quad (1)$$

R_0 was the initial sheet resistance, and R was the sheet resistance measured after rolling.

Fabrication and sintering of Cu and Cu/Sn metal-mesh TCFs. The Cu and Cu/Sn metal-mesh TCFs were prepared by our proprietary work²¹, and the fabrication process was presented in Supplementary Fig. S1. Firstly, the imprinting technology was used with the imprinting Ni master plate to form the mesh pattern on PET. Then Cu and Cu/Sn hybrid inks were filled into the trenches by blading. Finally, metal-mesh TCF was dried on a hot box at 80 °C for 2 min. The mesh pattern had a transmittance of 91% at 550 nm (as showed in Supplementary Fig. S3). Hexagonal trench structures were 3.5 μm in line width, 3 μm in depth and 74 μm in side length (Supplementary Fig. S5). By blading particle ink, the height of the metal grid was about 2.5–2.7 μm. The sintered energy density of Cu and Cu/Sn metal-mesh TCF from 4.66 J/cm² to 10 J/cm² was used, which was adjusted by changing the single pulse time with constant voltage of 2.6 kV. The sheet resistance of sintered Cu and Cu/Sn hybrid metal-mesh TCFs was measured by four-point probe station. Metal-mesh TCFs were characterized by the optical microscope (color 3D laser scanning microscope VK-9710, KEYENCE). The adhesion of Cu or Cu/Sn metal-mesh TCFs after sintering was tested according to the ASTM D3359 standard (An international standard)²⁴.

References

- Berggren, M., Nilsson, D. & Robinson, N. D. Organic materials for printed electronics. *Nat. Mater.* **6**, 3–5 (2007).
- Zhou, L. *et al.* High-performance flexible organic light-emitting diodes using embedded silver network transparent electrodes. *ACS Nano* **8**, 12796–12805 (2014).
- Dharmadasa, R., Jha, M., Amos, D. A. & Druffel, T. Room temperature synthesis of a copper ink for the intense pulsed light sintering of conductive copper films. *ACS Appl. Mater. Interfaces* **5**, 13227–13234 (2013).
- Xu, P. & Hamilton, M. C. Reduced-loss ink-jet printed flexible CPW with copper coating. *Ieee Microwave and Wireless Components Letters* **23**, 178–180 (2013).
- Allen, M. L., Jaakkola, K., Nummala, K. & Seppa, H. Applicability of metallic nanoparticle inks in RFID applications. *IEEE Trans. Compon. Packaging Technol.* **32**, 325–332 (2009).
- Kellomaki, T., Virkki, J., Merilampi, S. & Ukkonen, L. Towards washable wearable antennas: a comparison of coating materials for screen-printed textile-based UHF RFID tags. *Int. J. Antennas Propag.* **2012**, 1–11 (2012).
- Bidoki, S. M. *et al.* Inkjet printing of conductive patterns on textile fabrics. *AATCC Rev.* **5**, 11–14 (2005).
- Lee, H. M., Choi, S. Y., Jung, A. & Ko, S. H. Highly conductive aluminum textile and paper for flexible and wearable electronics. *Angew. Chem. Int. Edit.* **52**, 7718–7723 (2013).
- Cheng, Z. P. *et al.* Facile fabrication of ultrasmall and uniform copper nanoparticles. *Mater. Lett.* **65**, 3005–3008 (2011).
- Shin, D. H. *et al.* A self-reducible and alcohol-soluble copper-based metal-organic decomposition ink for printed electronics. *ACS Appl. Mater. Interfaces* **6**, 3312–3319 (2014).
- Jiang, H., Moon, K. S., Hua, F. & Wong, C. P. Synthesis and thermal and wetting properties of tin/silver alloy nanoparticles for low melting point lead-free solders. *Chem. Mat.* **19**, 4482–4485 (2007).
- Joo, M., Lee, B., Jeong, S. & Lee, M. Comparative studies on thermal and laser sintering for highly conductive Cu films printable on plastic substrate. *Thin Solid Films* **520**, 2878–2883 (2012).
- Perelaer, J., de Gans, B. J. & Schubert, U. S. Ink-jet printing and microwave sintering of conductive silver tracks. *Adv. Mater.* **18**, 2101–2104 (2006).
- Ryu, J., Kim, H. S. & Hahn, H. T. Reactive sintering of copper nanoparticles using intense pulsed light for printed electronics. *J. Electron. Mater.* **40**, 42–50 (2011).
- Chung, W.-H., Hwang, Y.-T., Lee, S.-H. & Kim, H.-S. Electrical wire explosion process of copper/silver hybrid nano-particle ink and its sintering via flash white light to achieve high electrical conductivity. *Nanotechnology* **27**, 205704–205716 (2016).
- Albrecht, A., Rivadeneyra, A., Abdellah, A., Lugli, P. & Salmerón, J. F. Inkjet printing and photonic sintering of silver and copper oxide nanoparticles for ultra-low-cost conductive patterns. *J. Mater. Chem. C* **4**, 3546–3554 (2016).
- Hecht, D. S., Hu, L. B. & Irvin, G. Emerging transparent electrodes based on thin films of carbon nanotubes, graphene, and metallic nanostructures. *Adv. Mater.* **23**, 1482–1513 (2011).
- Sam, F. L. M., Mills, C. A., Rozanski, L. J. & Silva, S. R. P. Thin film hexagonal gold grids as transparent conducting electrodes in organic light emitting diodes. *Laser Photon. Rev.* **8**, 172–179 (2014).

19. Kim, A., Won, Y., Woo, K., Kim, C. H. & Moon, J. Highly transparent low resistance ZnO/Ag nanowire/ZnO composite electrode for thin film solar cells. *ACS Nano* **7**, 1081–1091 (2013).
20. Hsu, P. C. *et al.* Performance enhancement of metal nanowire transparent conducting electrodes by mesoscale metal wires. *Nat. Commun.* **4**, 2522–2529 (2013).
21. Cui, Z. & Gao, Y. Hybrid printing of high resolution metal mesh as transparent conductor for touch panel and OLED Displays. *SID Int. Symp. Dig. Tec.* **46**, 398–400 (2015).
22. Mao, L. *et al.* Flexible silver grid/PEDOT:PSS hybrid electrodes for large area inverted polymer solar cells. *Nano Energy* **10**, 259–267 (2014).
23. Li, Y. W. *et al.* ITO-free photovoltaic cell utilizing a high-resolution silver grid current collecting layer. *Sol. Energy Mater. Sol. Cells* **113**, 85–89 (2013).
24. Wu, X. Z., Shao, S. S., Chen, Z. & Cui, Z. Printed highly conductive Cu films with strong adhesion enabled by low-energy photonic sintering on low-Tg flexible plastic substrate. *Nanotechnology* **28**, 11122–11127 (2017).
25. Cho, S. *et al.* Pressure-assisted electrode fabrication using simply synthesized Cu₃Sn alloy nanoparticles. *J. Mater. Chem. C* **3**, 2773–2777 (2015).
26. Collier, C. P., Vossmeier, T. & Heath, J. R. Nanocrystal superlattices. *Annu. Rev. Phys. Chem.* **49**, 371–404 (1998).
27. Jo, Y. H., Jung, I., Choi, C. S., Kim, I. & Lee, H. M. Synthesis and characterization of low temperature Sn nanoparticles for the fabrication of highly conductive ink. *Nanotechnology* **22**, 225701–225708 (2011).
28. Kim, Y. J., Ryu, C. H., Park, S. H. & Kim, H. S. The effect of poly (N-vinylpyrrolidone) molecular weight on flash light sintering of copper nanopaste. *Thin Solid Films* **570**, 114–122 (2014).
29. Hwang, H. J., Joo, S. J. & Kim, H. S. Copper nanoparticle/multiwalled carbon nanotube composite films with high electrical conductivity and fatigue resistance fabricated via flash light sintering. *ACS Appl. Mater. Interfaces* **7**, 25413–25423 (2015).
30. Jeong, S. *et al.* Controlling the thickness of the surface oxide layer on Cu nanoparticles for the fabrication of conductive structures by ink-jet printing. *Adv. Funct. Mater.* **18**, 679–686 (2008).
31. Nayral, C. *et al.* A novel mechanism for the synthesis of tin tin oxide nanoparticles of low size dispersion and of nanostructured SnO₂ for the sensitive layers of gas sensors. *Adv. Mater.* **11**, 61–63 (1999).
32. Joo, S. J., Hwang, H. J. & Kim, H. S. Highly conductive copper nano/microparticles ink via flash light sintering for printed electronics. *Nanotechnology* **25**, 265601–265611 (2014).
33. Albrecht, A., Rivadeneyra, A., Abdellah, A., Lugli, P. & Salmeron, J. F. Inkjet printing and photonic sintering of silver and copper oxide nanoparticles for ultra-low-cost conductive patterns. *J. Mater. Chem. C* **4**, 3546–3554 (2016).
34. Hwang, H. J., Oh, K. H. & Kim, H. S. All-photonic drying and sintering process via flash white light combined with deep-UV and near-infrared irradiation for highly conductive copper nano-ink. *Sci. Rep.* **6**, 19696–19705 (2016).
35. Dauskardt, R. H., Lane, M., Ma, Q. & Krishna, N. Adhesion and debonding of multi-layer thin film structures. *Eng. Fract. Mech.* **61**, 141–162 (1998).
36. Lauke, B. Determination of adhesion strength between a coated particle and polymer matrix. *Compos. Sci. Technol.* **66**, 3153–3160 (2006).
37. Yu, M.-H., Joo, S.-J. & Kim, H.-S. Multi-pulse flash light sintering of bimodal Cu nanoparticle-ink for highly conductive printed Cu electrodes. *Nanotechnology* **28**, 205205–205215 (2017).

Acknowledgements

This work was supported by the National Program on Key Research Project (No. 2016YFB0401500), the Strategic Priority Research Program of the Chinese Academy of Sciences (grant number XDA09020201), Science Foundation of Two sides of Strait (Key Program, No.U1605244), Program on Key Research Project of Jiangsu Province of China (No. BE2016173) and National Science Foundation of China (Grant No.51603228). The authors also thank Youth Innovation Promotion Association CAS (No. 2013206) for financial support.

Author Contributions

W.M. Su proposed the idea and conceived this study with X.L. Chen. X.L. Chen conducted the experiment and characterization with L.M. Xie and S.H. Nie. X.Z. Wu, S.S. Shao and Z. Chen prepared Cu nanoparticle ink. Z. Cui and J.Y. Zhuang revised the language. X.L. Chen wrote the manuscript and all the authors discussed the results.

Additional Information

Supplementary information accompanies this paper at <https://doi.org/10.1038/s41598-017-13617-4>.

Competing Interests: The authors declare that they have no competing interests.

Publisher's note: Springer Nature remains neutral with regard to jurisdictional claims in published maps and institutional affiliations.



Open Access This article is licensed under a Creative Commons Attribution 4.0 International License, which permits use, sharing, adaptation, distribution and reproduction in any medium or format, as long as you give appropriate credit to the original author(s) and the source, provide a link to the Creative Commons license, and indicate if changes were made. The images or other third party material in this article are included in the article's Creative Commons license, unless indicated otherwise in a credit line to the material. If material is not included in the article's Creative Commons license and your intended use is not permitted by statutory regulation or exceeds the permitted use, you will need to obtain permission directly from the copyright holder. To view a copy of this license, visit <http://creativecommons.org/licenses/by/4.0/>.

© The Author(s) 2017